Graphene in Catalysis

DOI: 10.1002/ange.201405669

Copper Nanoparticles Supported on Doped Graphenes as Catalyst for the Dehydrogenative Coupling of Silanes and Alcohols**

Juan F. Blandez, Ana Primo, Abdullah M. Asiri, Mercedes Álvaro, and Hermenegildo García**

Abstract: *Copper nanoparticles (NPs) supported on a series of undoped and doped graphene materials (Gs) have been obtained by pyrolysis of alginate or chitosan biopolymers, modified or not with boric acid, containing Cu^{2+} ions at 900 °C under inert atmosphere. The resulting Cu-G materials containing about 17 wt % Cu NPs (from 10 to 200 nm) exhibit high catalytic activity for the dehydrogenative coupling of silanes with alcohols. The optimal material consisting on Cu-(B)G is more efficient than Cu NPs on other carbon supports.*

Alcoxysilanes are high added-value commodity reagents for surface coating and modification[1–3] and for preparation of hybrid organic–inorganic materials.[4–6] One possibility for the synthesis of these reagents is the use of supported gold nanoparticles (NPs) as heterogeneous catalysts for the dehydrogenative coupling of silanes with alcohols (Scheme 1).[7–9]

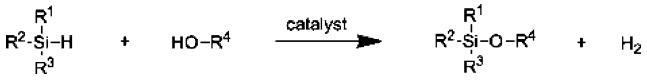

Scheme 1. Catalytic dehydrogenative *o*-silylation of alcohols by hydrosilanes.

One line of research of continued interest aims at replacing gold and precious metals by abundant and affordable base metals.[10–14] In this context, it is important to determine if the reaction shown in Scheme 1 can also be catalyzed by copper.

In addition to determine the catalytic activity of Cu, another point of this study is the use of graphene (G) as support. Carbonaceous materials are widely used as supports of metal NPs.[15,16] G is becoming increasingly used in catalysis as support of metal NPs.[17–19] G is a one-carbon-atom-thick layer of sp^2 carbon atoms in hexagonal arrangement, constituting the physical limit for 2D materials. G as support offers unique properties. Specifically, G has a very large specific surface area of about 2500 $m^2 g^{-1}$ totally accessible and the extended π orbitals on the G can interact strongly with the empty d orbitals of transition metal atoms at the interface. In addition, G can also adsorb substrates and reagents, bringing them near the active metal NPs. It has been observed that the activity of the metal NPs on G can be higher than on other supports because of the combination of the above effects.[20,21]

A third aspect of the present work is the innovative procedure reported here for the simultaneous preparation of Cu NPs on G by carbonization of natural biopolymers. The procedure also allows doping or co-doping of the G sheet with heteroatoms. The interaction of metal NPs with heteroatoms on doped G has been proposed from theoretical calculations as a tool to control the activity of G.[22] The resulting graphitic material, after exfoliation, exhibits high activity for the dehydrogenative coupling of silanes with alcohols (Scheme 1).

The preparation method for the series of Cu-G materials is summarized in Scheme 2. It starts with an aqueous solution of biopolymer (alginate or chitosan) modified or not by boric acid that is precipitated with a Cu^{2+} salt. The resulting Cu^{2+}-modified biopolymer hydrogel is dried and submitted to pyrolysis at 900 °C under inert atmosphere to render a Cu-containing graphitic carbon residue. During the pyrolysis under reductive conditions, Cu^{2+} undergoes spontaneous reduction to Cu^0 forming Cu NPs, simultaneously to graphitization of the biopolymer. Pyrolysis of alginate and other natural polysaccharides form graphitic carbon residues that can be easily exfoliated into G sheets.[23–25] In the case of chitosan, a polysaccharide of glucosamine, the resulting graphitic residue contains 7 wt % of N, according to combustion analysis. If the biopolymer contains boric acid, then, the resulting graphitic residue becomes doped with boron.[23] Sonication of the Cu-containing graphitic carbon residue

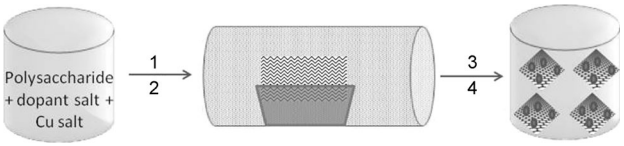

Scheme 2. Preparation procedure for the present Cu-G materials. The polysaccharide can be alginate or chitosan. The dopant salt can be borate. 1) Gelification of biopolymers by Cu^{2+}, 2) pyrolysis at 900 °C in Ar 3) graphitization and 4) ultrasonication.

[*] J. F. Blandez, Dr. A. Primo, Prof. M. Álvaro, Prof. H. García
Instituto de Tecnología Química and
Chemistry Department (UPV-CSIC)
Avda/de los Naranjos s/n 46022 Valencia (Spain)
E-mail: hgarcia@qim.upv.es
Prof. A. M. Asiri, Prof. H. García
Center of Excellence for Advanced Materials Research
King Abdulaziz University, Jeddah (Saudi Arabia)

[**] Financial support by the Spanish Ministry of economy and competitiveness (Severo Ochoa and CTQ2012-32315) and Generalitat Valenciana Prometeo 2012-013) is gratefully acknowledged.
Supporting information for this article is available on the WWW under http://dx.doi.org/10.1002/anie.201405669.

leads to suspended Cu-G and Cu-doped G. The list of materials prepared and their main analytical data are presented in Table S1 (see the Supporting Information).

The obtained Cu-graphitic carbon atoms were characterized by chemical analysis, XRD, and electron microscopy. The Cu content on the materials was determined by ICP-AAS (see Table S1).

Because of the high Cu percentage and its crystallinity arising from the high pyrolysis temperature, the samples Cu-graphitic carbon exhibit an intense X-ray diffractogram (Figure S9), corresponding to the (1.0.0), (2.0.0), and (2.2.0) Cu facets, without observation of any peak of graphitic carbon.

Sonication in *n*-butanol of the Cu-graphitic carbon atoms leads to persistent inks where graphitic platelets were suspended. After removal the residual non/dispersed solid residue (typically about 20% of the initial weight), the suspended material was characterized by microscopy. TEM shows a 2D morphology of micrometric length with the presence of wrinkles because of the flexibility of the G layers. The presence of Cu-NPs was also observed (Figure 1). Statistical analysis of the size distribution indicates that Cu NPs show a broad range of particle sizes from 10 to 200 nm (Figures S1–S4). The average particle diameter of Cu NPs for Cu-G was 24 ± 7 nm. It was found that the G samples containing nitrogen as dopant element exhibit larger average size Cu NPs. This range of Cu particle dimension is remarkable considering that the samples were obtained by pyrolysis at 900 °C. It is very likely that the biopolymers and the carbon residues derived from them, control the growth of Cu NPs during the pyrolysis as it has been proposed for metal oxides.[26–29] Cu NPs appear well-dispersed on G having a round morphology. In addition the presence of nanometric holes on the sheet can also be observed (see Figure 1). These holes could be formed by CO_2 evolution during pyrolysis and could play a role on the stabilization of metal NPs and on the catalytic activity of Gs.[30]

The single layer morphology for some platelets was determined by AFM. Figure 2 shows a view of some of these platelets for Cu-(B)G, with the count of the average height of Cu NPs from 10 to 25 nm and the vertical height corresponding to a single layer (B)G.

Raman spectroscopy of Cu NPs supported on graphitic carbon residues shows the expected 2D, G, and D peaks at 2700, 1590, and 1350 cm^{-1}, respectively. The intensity ratio of the G and D peaks varied from 1.3 to 1.6. It should be noted that the presence of dopant elements is reflected in Raman spectroscopy by increasing D band intensity.

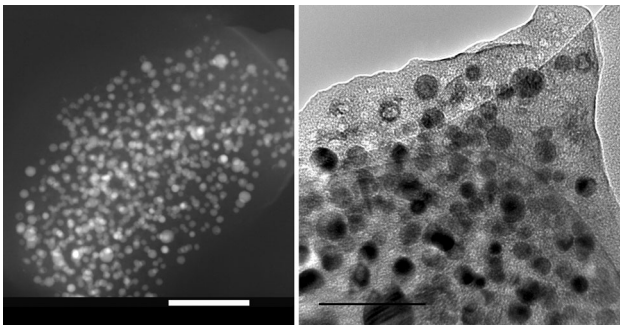

Figure 1. Dark field scanning TEM image (left; scale bar = 200 nm) and TEM image of Cu-G (right; scale bar = 100 nm).

X-ray photoelectron spectroscopy (XPS) determines the composition of the Cu NPs supported on G and the distribution of each element in different oxidation states. Depending on the sample, the C1s peak can be deconvoluted in three or four component, the major one appearing at 284.5 eV characteristic of sp^2 G carbon atoms. Other components of C1s appear at higher binding energy and correspond to C atoms bonded to the dopant element and oxygen. C atoms

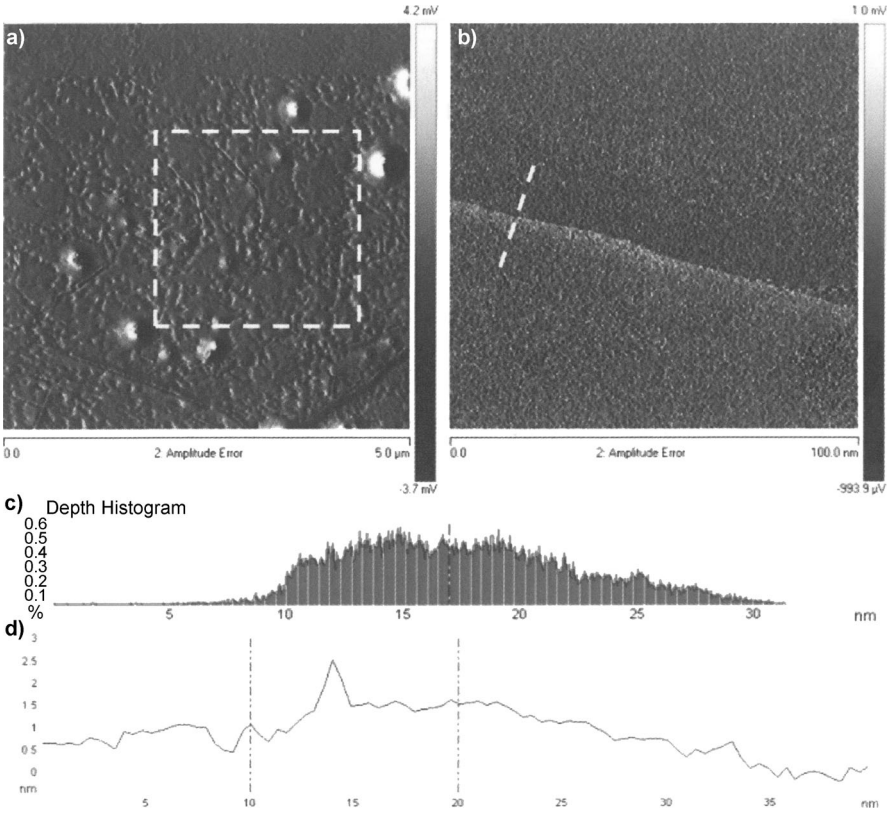

Figure 2. AFM images of Cu-(B)G (a and b). Panel (a) presents a top AFM view of Cu-(B)G with a 2.5×2.5 μm^2 area where the height of the Cu NPs was measured. Panel (b) presents higher magnification of the (B)G sheet (lower part of the image) at the border and the dashed line indicates the points through which the vertical height of the sheet was measured. Panel (c) shows the height distribution (*x* axis) of Cu NPs inside the square delimited in panel (a). Panel (d) shows the height variations along the white line in panel (b).

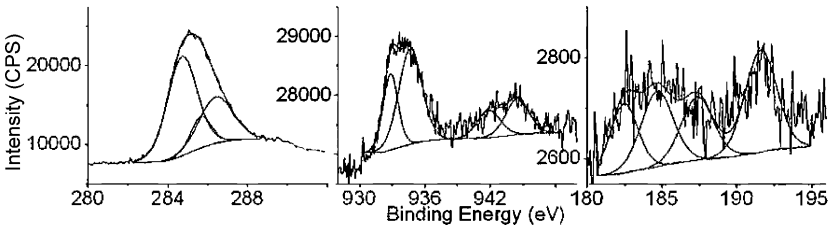

Figure 3. XPS peaks recorded for the Cu-(B)G sample and the best deconvolution into individual components.

associated to dopant elements or at defects, are in a proportion that agrees with the percentage of dopant element. Table S1 summarizes the percentage for each component in the corresponding XPS peaks of each sample.

As expected, depending on the sample, the presence in XPS of the peak corresponding to the dopant element, either boron, nitrogen or both was also detected. Figure 3 shows the XPS peaks corresponding to the three elements present in Cu-(B)G (see also Figures S12 and S13 for additional XPS). The intensity of the XPS peak for each element and the corresponding response factor allowed determination of the elemental composition of the sample. In addition, the 2p3/2 peak corresponding to Cu was also observed for all the samples with very similar binding energy. Deconvolution of the Cu2p3/2 peak allows the determination of the atomic proportion of Cu^{II} with respect to the combined amount of Cu^{0} and Cu^{I}. Overall, the above characterization provides firm evidence of the success on the formation of Cu NPs simultaneously with the synthesis of doped Gs. Thus, chemical analysis and XPS detect the presence of the expected elements, while the morphology and crystallinity of G were determined by microscopy. AFM shows that sonication produces exfoliation of the graphitic carbon atoms to single- or few-layer platelets.

The purpose of this work is to study the catalytic activity of Cu NPs supported on Gs. Besides showing that Cu NPs are active for the dehydrogenative coupling of silane and alcohols, another aspect is to show how doping alters the activity of G.

In the initial stage of our work we selected as model reaction the coupling of dimethylphenylsilane (**1a**) with *n*-butanol (**2a**). A preliminary screening to establish the efficiency of the series of Cu-containing catalysts was carried out at various temperatures. The only compound observed was butoxydimethylphenylsilane (**3a**). Particularly notable is the absence of the disiloxane. The results obtained are presented in Table 1, while the time–conversion plots for representative experiments are shown in Figure 4. In those experiments where the selectivity was low (see footnote [c] in Table 1), the reason was silane adsorption on G, making low the mass balances (see Figure S12).

The presence of dopant elements exhibits a remarkable influence on the catalytic activity, the most efficient catalyst being Cu-(B)G followed by Cu-G. In view of the previous particle size characterization, the most likely explanation for this performance is the larger particle size of Cu NPs for those G samples having N as dopant element (compare particle sizes in Figures S1–S4). Under optimal conditions measured for an experiment using ten times higher amount of **1a** and **2a** a minimum turnover number (TON) of 2000 with a turnover frequency (TOF) of 4.16 h^{-1} was obtained for Cu-(B)G. The initial reaction rate of Cu-G was higher than that of Cu-(B)G, but the conversion of **1a** in the presence of Cu-G levels off earlier than for Cu-(B)G. One explanation is faster deactivation of Cu-G compared to Cu-(B)G.

Table 1: Dehydrogenative coupling of dimethylphenylsilane (**1a**) and *n*-butanol (**2a**) in the presence of Cu-containing catalysts.[a]

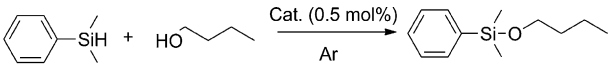

1a **2a** **3a**

Entry	Catalyst	Conditions [°C]	Conversion [%][b]	Selectivity [%][b]
1	Cu-G	sonication, RT	28	32[c]
2	Cu-(B)G	sonication, RT	33	21[c]
3	Cu-G	80	74	93
4	Cu-(B)G	80	47	92
5	Cu-(B,N)G	80	47	87
6	Cu-G	100	80	95
7	Cu-(B)G	100	100[c]	100[d]
8	Cu-(B,N)G	100	51	43[c]
9	Cu-(N)G	100	65	80

[a] Reaction conditions: **1a** (5 mmol), **2a** (10 mmol), catalyst (0.5 mol%), Ar atmosphere, 24 h. [b] Conversion and selectivity were determined by GC using internal standard. [c] Incomplete mass balance because of adsorption is responsible for the low selectivity. [d] 48 h.

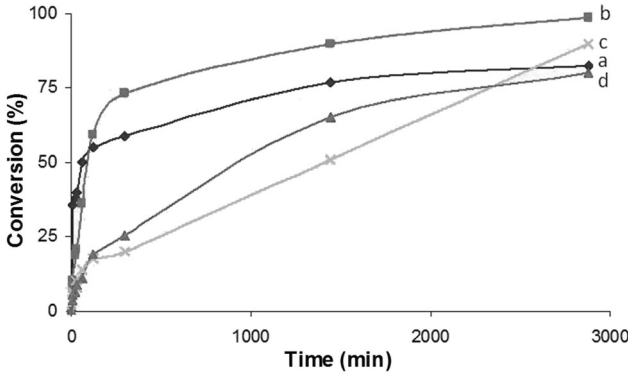

Figure 4. Time–conversion plot for the reaction of **1a** and **2a** in the presence: Cu-G (a), Cu-(B)G (b), Cu-(B,N)G (c), and Cu-(N)G (d).

To address this issue we performed twin experiments in which the reaction of **1a** and **2a** were carried out in the presence of Cu-G and after 1500 minutes an additional amount of Cu-G was added in one of them (see Figure S13). While the reaction in which no fresh Cu-G was added did not progress further, the twin experiment adding fresh Cu-G catalyst re-start increasing the conversion, reaching 92% at 3000 minutes. This experiment clearly evidences faster deactivation of Cu-G during the reaction than that of Cu-(B)G. This deactivation is

likely to be due to product adsorption, in view of the reusability tests. In the case of Cu-(B)G a kinetic study of product deactivation showed that the time–conversion plots were not influenced by the presence of **3a** in the range from 0 to 0.4 M (Figure S13).

The activation energy (E_a) of the dehydrogenative coupling of **1a** and **2a** was determined by carrying out this reaction in the range of temperatures from 40 until 100 °C, determining the initial reaction rate from the slope of the time conversion plot at zero reaction time. E_a was obtained from the best fit of the logarithm of the reaction rate versus the inverse of the absolute temperature, giving 27.7 ± 0.3 kJ mol^{-1} (see Figure S14). This value for E_a is relatively low indicating that Cu NPs are efficient catalysts. Because of the low E_a value, the possibility that the reaction could be limited by diffusion was considered and dismissed, since a series of experiments in which the stirring rate was set at 600 and 1200 rpm did not show any difference in the time–conversion plot (see Figure S18).

To compare the activity of Cu NPs on G, we screened the activity of a series of Cu-containing catalysts on various supports including different carbon materials (diamond NPs and high-surface-area-active carbon atoms) as well as on organic biopolymer (chitosan) and metal oxide (MgO) (see the Supporting Information for relevant data of these catalysts).

The activity data for the reaction of **1a** and **2a** catalyzed by various Cu-containing catalysts is summarized in Table 2.

Table 2: Results of the dehydrogenative coupling of silane **1a** with *n*-butanol **2a** catalyzed by Cu NPs supported on different solids.[a]

Entry	Catalyst	Conversion [%][b]	Selectivity [%][b]
1	Cu-G	80	95
2	Cu-Diamond NPs	89	26
3	Cu-Silylated Diamond	44	6
4	Cu/MgO	20	29
5	Cu/chitosan	94	9
6	Cu/active carbon		
	first use	99	44
	second use	30	<5

[a] Reaction conditions: **1a** (5 mmol), **2a** (10 mmol), catalyst (0.5 mol%), Ar atmosphere, 100 °C, 24 h. [b] Conversion and selectivity determined by GC with internal standard.

While the activity of supported Cu NPs as catalysts for the dehydrogenative coupling is general, the selectivity of the process is low or moderate, because of the competitive formation of disiloxane as the major product. In the case of Cu/active carbon that shows a moderate selectivity, the activity fades in the second use because of Cu leaching. As a summary of Table 2, the combination of Cu NPs and G as support renders the best performing material, showing the advantage of G as support.

To provide a valid comparison of the selectivity of various catalysts, selectivity values should be compared at similar conversion. In the present case, it was, however, observed that for Cu NPs supported on G selectivity was almost constant with conversion (see Figure S19) and no other products are observed. Only adsorption is responsible for some apparent decrease in selectivity. Thus, observation of disiloxane formation in entries 2 to 6 in Table 2 indicates the superiority of G as support for this reaction.

Reusability of Cu-(B)G and catalyst stability was tested by performing a series of three consecutive runs using the same sample recovered by filtration, washed with hexane, and redispersed by sonication. It was observed that conversion of **1a** decreased from 87 to 74 and 51% from the first to the second and third use, respectively (see Figure S20). This indicates a gradual deactivation of Cu-(B)G upon use. TEM images of the three times used Cu-(B)G do not show agglomeration of Cu NPs (see Figure S.21 in SI) although it is a common cause of deactivation. In fact, the average Cu NP size of the used catalyst is even smaller. In contrast, surface area determination in the liquid phase using methylene blue as probe shows a significant decrease in the surface area from 1527 to 1014 m^2 g^{-1}. Analysis of Cu in *n*-butanol after the reaction indicates Cu leaching to some extent. Thus, at present, the most likely causes for the gradual catalyst deactivation seem to be the partial stacking of (B)G layers and leaching of Cu from (B)G to the solution.

In view of the high activity of Cu-(B)G as catalyst for the coupling of **1a** and butanol (see Table 1, entry 4), we proceeded to study the scope of this catalyst for other silanes and alcohols. The results obtained are presented in Table 3.

Table 3: Activity data for the dehydrogenative coupling of silanes and alcohols catalyzed by Cu-(B)G.[a]

Entry	Silane	Alcohol	*t* [h]	*T* [°C]	Conver. [%][b]	Selec. [%][b]
1	Me_2PhSiH	BuOH	48	100	>99	>99
2	Me_2PhSiH	MeOH	24	70	69	90
3	Me_2PhSiH	EtOH	24	70	54	94
4	Ph_2SiH_2	BuOH	0.5	100	>99	100
5	Ph_2SiH_2	MeOH	1	70	>99	100
6	Ph_2SiH_2	EtOH	1	70	>99	100
7	$PhSiH_3$	BuOH	0.5	100	>99	100
8	$PhSiH_3$	MeOH	1	70	>99	100
9	$PhSiH_3$	EtOH	5	70	90	93

[a] Reaction conditions: **1** (5 mmol), **2** (entries 1–3: 10 mmol, entries 4–6: 20 mmol; entries 7–9: 30 mmol), catalyst (0.5 mol%), Ar atmosphere; [b] The selectivity and the conversion were obtained by GC with internal standard.

As expected, using Cu-(B)G high to moderate conversions were achieved with excellent selectivity towards the target alcoxysilane.

As it can be seen in Table 3, the dehydrogenative coupling can also be performed using methanol or ethanol as alcohols. In these cases, however, because of their lower boiling point compared to *n*-butanol, the reaction was carried out at lower temperature and, for this reason, the conversion of silane **1a** was significantly lower than that achieved at the same time for *n*-butanol at higher temperature. Comparing methanol and ethanol, the first was more reactive probably because of steric effects.

Besides dimethylphenylsilane, other silanes were also tested. Diphenylsilane reacts much faster than dimethylphe-

nylsilane affording in a very short period of time the dialcoxy product (Table 3, entry 4). This silane also reacts with methanol and ethanol to the corresponding diethoxy and dimethoxy products, although longer reaction times are needed because of the lower reaction temperature (Table 3, entries 5 and 6). In these cases, the evolution of the reaction mixture shows the presence of low concentrations of the corresponding monoalcoxysilane that appears as primary but instable product. Phenylsilane also reacts promptly with *n*BuOH, MeOH, and EtOH to the corresponding trialcoxy phenylsilane (Table 3 entries 7, 8, and 9). Also in these cases, the formation of intermediates of the corresponding mono- and dialcoxy phenylsilanes was observed. Apparently, the reactivity of silanes increases as the number of Si–H bonds increases.

Based on the results obtained and the nature of the catalyst, a reasonable mechanistic proposal is that silane interacts with Cu NPs to form Cu-Si and Cu-H species, while the alcohol interacts with Lewis acid sites on G leading to chemisorption with formation of alcoxide and protons. Preliminary FTIR measurements of *n*-butanol adsorption on Cu-(B)G show the presence of a band at about 1050 cm^{-1} upon contacting *n*-butanol at 80 °C that disappears subsequently upon further heating. This absorption band could be attributed to the alcoxide interacting with the (B)G sheet. The coupling between the silyl group bonded to Cu and the alcoxide on the Lewis acid on G will render the final product (Scheme 3). The primary role of the dopant element on the

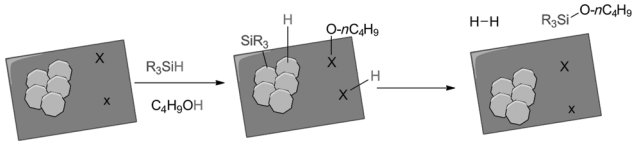

Scheme 3. Pictorial illustration of Cu NPs supported on doped G sheets. Activation of Si–H bonds of silane would take place on Cu NPs, while the G sheet would cooperate by adsorbing the alcohol. This adsorption could take place preferentially on the dopant elements (indicated as X).

catalytic activity seems to be the control of the Cu particle size distribution as previously proposed when commenting the TEM images, but also should participate in adsorption of reagents and products (see Figure S14) and probably also in other steps in the reaction mechanism. The combined information of in situ spectroscopic techniques and computational calculations are necessary to gain deeper insight into the influence of dopants elements in the catalyst activity.

Thus, in the present study we have shown that Cu NPs supported on G materials are efficient catalysts for the dehydrogenative coupling of silanes and alcohols. Pyrolysis of a conveniently modified biopolymer containing Cu^{2+} leads to the simultaneous formation of doped graphitic carbon residues and Cu NPs. The solid can be easily exfoliated by sonication. Doping of G exhibits a notable influence on the catalytic activity. Comparison with other types of carbon atoms containing Cu indicates that G exhibits a superior performance than other supports that can be derived from the large surface area, high adsorption capacity and strong metal–G interaction.

Experimental Section

Cu NPs supported on Gs were prepared in a single step starting from commercial alginate or chitosan that were precipitated with $Cu(NO_3)_2$ and submitted subsequently to pyrolysis and exfoliation as indicated in the supporting information. The preparation of the catalysts included in Table 2 is also described in the Supporting Information. An example to illustrate the procedure is included here.

Synthesis of Cu/G: Alginic acid sodium salt from brown algae (0.5 g, Sigma) was dissolved in a 50 mL of $Cu(NO_3)_2$ aqueous solution (1 wt % with respect to the alginic acid sodium salt). Before pyrolysis, the solution was concentrated by heating in an oven at 100 °C overnight. The pyrolysis was performed in an electrical horizontal tubular oven in an argon stream (50 mL min^{-1}) using the following oven program: 200 °C during 2 h for annealing and then heating at 10 °C min^{-1} up to 900 °C for 6 h. This graphitic carbon residue is sonicated at 700 W during 1 h for obtaining the dispersed Cu/G in the reaction mixture.

General catalytic procedure for the dehydrogenative silylation with alcohols: The catalyst (0.5 mol %) was charged in a 5 mL reinforced glass reactor equipped with a magnetic bar. Then, alcohol was added (2–4 mmol) and the reactor was sonicated under dry N_2 atmosphere to deoxygenate. Finally, the silane was introduced in the reactor with a syringe. The reaction was stirred at 100 °C or the required temperature from 30 minutes to 48 h, depending on the substrates, in an oil bath. The reaction mixture was allowed to cool to room temperature and the catalyst removed by filtration. For GC analysis, a known amount of dodecane as internal standard was added. Products were purified by flash chromatography on silica gel with anhydrous ethyl acetate/hexane mixture and were characterized by the spectroscopic techniques (see the Supporting Information for spectroscopic data).

Received: May 27, 2014
Revised: July 24, 2014
Published online: September 5, 2014

Keywords: alcoxysilanes · dehydrogenative coupling · graphene · heterogeneous catalysis · metal nanoparticles

[1] P. G. Belelli, M. L. Ferreira, D. E. Damiani, *J. Mol. Catal. A* **2000**, *159*, 315.
[2] I. Díaz, J. Perez-Pariente, *Chem. Mater.* **2002**, *14*, 4641.
[3] M. Matheron, T. Gacoin, J. P. Boilot, A. Bourgeois, A. Brunet-Bruneau, J. Rivory, A. Jimenez, J. Biteau, *Stud. Surf. Sci. Catal.* **2005**, *156*, 327.
[4] A. Gómez-Avilés, P. Aranda, F. M. Fernandes, C. Belver, E. Ruiz-Hitzky, *J. Nanosci. Nanotechnol.* **2013**, *13*, 2897.
[5] N. N. Herrera, J. M. Letoffe, J. L. Putaux, L. David, E. Bourgeat-Lami, *Langmuir* **2004**, *20*, 1564.
[6] M. Jaber, F. O. M. Gaslain, J. Miehe-Brendle, *Clays Clay Miner.* **2009**, *57*, 35.
[7] H. García, M. Stratakis, *Chem. Rev.* **2012**, *112*, 4469.
[8] T. Mitsudome, Y. Yamamoto, A. Noujima, T. Mizugaki, K. Jitsukawa, K. Kaneda, *Chem. Eur. J.* **2013**, *19*, 14398.
[9] T. Taguchi, K. Isozaki, K. Miki, *Adv. Mater.* **2012**, *24*, 6462.
[10] S. Rendler, O. Plefka, B. Karatas, G. F. Auer, R. C. Muck-Lichtenfeld, S. Grimme, M. Oestreich, *Chem. Eur. J.* **2008**, *14*, 11512.
[11] K. T. Kira, H. A. Hamajima, T. Baba, S. Takai, M. Isobe, *Tetrahedron* **2002**, *58*, 6485.

[12] J. W. Park, C. H. Jun, *Org. Lett.* **2007**, *9*, 4073.
[13] H. S. Hilal, A. Rabah, I. S. Khatib, A. F. Schreiner, *J. Mol. Catal.* **1990**, *61*, 1.
[14] H. Ito, K. Takagi, T. Miyahara, M. Sawamura, *Org. Lett.* **2005**, *7*, 3001.
[15] J. A. Zazo, J. A. Casas, A. F. Mohedano, J. J. Rodríguez, *Appl. Catal. B* **2006**, *65*, 261.
[16] S. Ikeda, S. Ishino, T. Harada, N. Okamoto, T. Sakata, H. Mori, S. Kuwabata, T. Torimoto, M. Matsumura, *Angew. Chem. Int. Ed.* **2006**, *45*, 7063; *Angew. Chem.* **2006**, *118*, 7221.
[17] P. V. Kamat, *J. Phys. Chem. Lett.* **2010**, *1*, 520.
[18] C. Xu, X. Wang, J. Zhu, *J. Phys. Chem. C* **2008**, *112*, 19841.
[19] L. Shang, T. Bian, B. Zhang, D. Zhang, L. Z. Wu, C. H. Tung, Y. Yin, T. Zhang, *Angew. Chem. Int. Ed.* **2014**, *53*, 250; *Angew. Chem.* **2014**, *126*, 254.
[20] T. Sun, Z. Zhang, J. Xiao, C. Chen, F. Xiao, S. Wang, Y. Liu, *Nature* **2013**, *493*, 195.
[21] E. Yoo, T. Okata, T. Akita, M. Kohyama, J. Nakamura, I. Honma, *Nano Lett.* **2009**, *9*, 2255.
[22] J. Ding, M. Wang, X. Zhang, C. Ran, *RSC Adv.* **2013**, *3*, 14073.
[23] A. Dhakshinamoorthy, A. Primo, P. Concepcion, M. Alvaro, H. Garcia, *Chem. Eur. J.* **2013**, *19*, 7547.
[24] M. Latorre-Sánchez, A. Primo, H. García, *Angew. Chem. Int. Ed.* **2013**, *52*, 11813; *Angew. Chem.* **2013**, *125*, 12029.
[25] I. Lazareva, Y. Koval, M. Alam, S. Strömsdörfer, P. Müller, *Appl. Phys. Lett.* **2007**, *90*, 262108.
[26] M. Buaki-Sogo, M. Serra, A. Primo, M. Alvaro, H. García, *ChemCatChem* **2013**, *5*, 513.
[27] A. El Kadib, A. Primo, K. Molvinger, M. Bousmina, D. Brunel, *Chem. Eur. J.* **2011**, *17*, 7940.
[28] A. El Kadib, K. Molvinger, T. Cacciaguerra, M. Bousmina, D. Brunel, *Microporous Mesoporous Mater.* **2011**, *142*, 301.
[29] C. Lavorato, A. Primo, R. Molinari, H. Garcia, *ACS Catal.* **2014**, *4*, 497.
[30] P. Shi, R. Su, F. Wan, M. Zhu, D. Li, S. Xu, *Appl. Catal. B* **2012**, *123–124*, 265.